ELSEVIER

Catalysis Today 72 (2002) 133–144

CATALYSIS TODAY

www.elsevier.com/locate/cattod

Microstructural comparison of calcined and uncalcined gold/iron-oxide catalysts for low-temperature CO oxidation

N.A. Hodge [a], C.J. Kiely [a,b,*], R. Whyman [b], M.R.H. Siddiqui [b], G.J. Hutchings [c], Q.A. Pankhurst [d], F.E. Wagner [e], R.R. Rajaram [f], S.E. Golunski [f]

[a] *Department of Materials Science and Engineering, University of Liverpool, Merseyside L69 3BX, UK*
[b] *Department of Chemistry, University of Liverpool, Merseyside L69 7ZD, UK*
[c] *Department of Chemistry, University of Wales-Cardiff, P.O. Box 912, Cardiff CF10 3TB, UK*
[d] *Department of Physics, University College London, Gower Street, London W1CE 6BT, UK*
[e] *Physik Department, Technische Universitat Munchen, D-85747 Garching, Germany*
[f] *Johnson Matthey Technology Centre, Blount's Court, Sonning Common, Reading RG4 9NH, UK*

Abstract

A series of gold/iron-oxide catalysts has been prepared by an inverse co-precipitation method from a mixture of $HAuCl_4 \cdot 3H_2O$ and $Fe(NO_3)_3 \cdot 9H_2O$. Samples calcined at 400 °C for 3 h exhibited poor activity towards CO oxidation, whereas uncalcined materials that had only been dried at 120 °C for 16 h exhibited a far superior catalytic activity. The most active material of this latter type is shown to have 100% CO conversion at 20 °C for at least 10 h. Detailed characterisation of the dried and the calcined materials using ICP and BET analysis, XRD, HREM, STEM-EDX and Mössbauer spectroscopy has shown significant differences in their microstructure. The dried materials consist of micron scale agglomerates of 4–8 nm disordered $Fe_5HO_8 \cdot 4H_2O$ particles on which the Au is uniformly dispersed in the form of a mixture $AuOOH \cdot xH_2O$ and Au^0. By comparison, the calcined materials are comprised solely of 3–5 nm cuboctahedral metallic Au particles supported on 20 nm diameter well-crystalline α-Fe_2O_3 particles. Our microstructural observations and catalytic measurements are discussed in the context of the Bond–Thompson mixed Au^{x+}/Au^0 model for the low-temperature CO oxidation catalyst.

Keywords: Low-temperature CO oxidation; Au–MO; Au oxyhydroxide; Ferrihydrite

1. Introduction

Materials produced when Au is immobilised over a range of metal-oxide supports have emerged over recent years as very active systems for low-temperature CO oxidation. Haruta et al. [1,2] stimulated interest in this area by reporting a co-precipitation technique for depositing nanosized Au particles on metal-oxide supports, and producing materials which exhibited high catalytic activity for the oxidation of CO at temperatures below 0 °C. It was suggested that a synergistic mechanism occurs at the gold- and metal-oxide interface, with the metal-oxide not simply acting as an inert carrier, but playing a necessary part of the catalytic process [3,4]. CO oxidation was proposed to occur when CO absorbs onto a metallic Au site adjacent to a metal-oxide site occupied by an adsorbed O_2 molecule, with the catalytic reaction proceeding via an intermediate carbonate-like species that decomposes

* Corresponding author. Present address: Department of Materials Science and Engineering, University of Liverpool, Merseyside L69 3BX, UK.
E-mail address: kiely@liv.ac.uk (C.J. Kiely).

0920-5861/02/$ – see front matter
PII: S0920-5861(01)00487-4

to CO_2 when it desorbs from the surface. Following this line of reasoning, a high dispersion of 2–3 nm diameter Au particles on the metal-oxide support should represent an optimised catalyst because the line length of 'active' interfacial perimeter between particle and support would then be maximised.

In a recent review [5] of the rapidly expanding literature based on the Au catalysed oxidation of CO, Bond and Thompson noted that there is a general consensus emerging that the preparation route, catalyst pre-treatment conditions, the choice of support and the Au particle size all have a significant influence on the ultimate catalytic performance. They also pointed out a number of issues where further work is required to clarify apparent contradictions in the literature. In particular, it is still uncertain whether the catalytically active Au entities are zerovalent atoms or oxidised Au species (e.g. Au^{III}). FTIR studies of chemisorbed CO on these catalysts suggest the simultaneous existence several different types of Au species including Au^0 in high or low co-ordination, and 'positively polarised' gold atoms at the particle periphery [6,7]. Au oxidation state data from various EXAFS and XPS experiments are less conclusive because the vacuum or irradiation conditions employed during the experimental measurements may themselves alter the oxidation state of the metal. Although many authors are quite polarised in their views that *only* Au^0 or *only* Au^{x+} species are responsible for catalytic activity, some highly plausible new models have been recently suggested [5,8,9] whereby *both* species are simultaneously present and play an active role in the catalytic process. Bond and Thompson [5] suggest that the Au^{x+} ions exist as a two-dimensional layer at the Au/metal-oxide interface which acts as a 'chemical glue' that binds the particle to the support [10]. Consequently, a peripheral ring of Au^{x+} ions is envisaged which facilitates separation of Au^0 from the oxide support. In this new model, a CO molecule initially chemisorbed on Au^0 is attacked by a hydroxyl group fixed to a Au^{x+} ion, forming a carboxylate group attached to the periphery. This is in turn attacked by a superoxide ion from the support, which must be responsible for oxidising two carboxylate ions; thus liberating the OH^- ion to re-engage in the catalytic cycle. It is also pointed out that the exact Au^{x+}/Au^0 ratio may change during: (i) calcination in air, (ii) reduction under hydrogen or, and (iii) even during the initial stages of reaction.

Adding further to this particular controversy are some recent studies by our research group [11,12] of Au supported on ferric-oxide, where the poorly ordered uncalcined precursor material was found to be considerably more active for low-temperature CO oxidation than the calcined materials which should exhibit the 'classic' 3–4 nm Au particles supported on α-Fe_2O_3. On the basis of XRD and Mössbauer spectroscopy measurements, the uncalcined material has been tentatively proposed to consist primarily of $AuOOH{\cdot}xH_2O$ supported on a ferrihydrite phase. In this work, we have performed a repeat preparation of these Au/ferric-oxide samples and have carried out a more thorough structural characterisation of both the calcined and uncalcined materials using ICP and BET analysis, XRD, HREM, STEM-EDX mapping and Mössbauer spectroscopy. Our observations are correlated with low-temperature CO oxidation catalytic measurements and the results are discussed in the context of the Bond–Thompson mixed Au^{x+}/Au^0 model for the catalyst.

2. Experimental

2.1. Sample preparation

A series of three Au/ferric-oxide catalyst precursors with nominal Au contents ranging between 1 and 2.5 at.%, were prepared using an inverse co-precipitation technique from 'as supplied' commercial reagents. Dilute aqueous solutions of $HAuCl_4{\cdot}3H_2O$ and $Fe(NO_3)_3{\cdot}9H_2O$ were mixed together with vigorous stirring (400 rpm) at 50 °C. Aqueous Na_2CO_3 (0.25 mol l^{-1}) was then added drop-wise until a solution of pH = 8.2 was attained. The resulting precipitate was then immediately recovered by filtration and washed with 1 l of warm (50 °C) deionised water. The product, once dried for ~16 h at 120 °C, was ground to a fine powder prior to pelleting at a pressure of 10 t. The pellets were crushed and sieved to the required mesh size for testing in the microreactor (150–250 μm). Portions of the sieved materials were calcined at 400 °C for 3 h in static air.

2.2. Catalytic activity measurements

The materials dried at 120 °C as well as the calcined catalysts were tested for CO oxidation using a

fixed bed laboratory microreactor under standard conditions [11]. Typically, CO (5% in He, 5 ml min^{-1}) and O_2 (50 ml min^{-1}) were fed to the reactor at controlled feed rates using mass flow controllers, passed over the catalyst (50 mg) at 20 °C, and the products were analysed using on-line gas chromatography.

2.3. ICP and BET analysis

Inductively coupled plasma analysis was performed on a Perkin-Elmer II ICP-AES spectrometer, using approximately 2.5 mg of sample dissolved in 1–5 ml of aqua regia, made up to 100 ml with deionised water. BET measurements were carried out using a computer controlled ASAP 200 Micrometrics Surface Area Analyser. Prior to adsorption measurements, the samples were degassed under a vacuum of 5 μl Hg at 100 °C for 2 h.

2.4. X-ray diffraction

The powder diffractometer employed in this study was an Enraf Nonius FR590 X-ray generator employing a Cu Kα source. The diffractometer was fitted with an Inel CPS 120 hemispherical detector that allowed all angles to be measured simultaneously. The finely powdered samples were compressed into a metal sample holder that was rotated about an axis normal to its plane during exposure to X-rays so as to randomise the orientation of the crystallites. Patterns were obtained in the range $2\theta = 5$–127°, with measurements taken at 0.03° intervals.

2.5. Electron microscopy

Powder samples for electron microscopy examination were dispersed in a dry state onto a holey carbon film supported on a 3.05 mm diameter Cu mesh grid. High resolution electron microscopy (HREM) was performed in a JEOL 2000EX microscope operating at 200 kV. Chemical microanalysis was carried out in a VG HB 601 Scanning Transmission Electron Microscope operating at 100 kV and equipped with a Link systems EDX spectrometer.

2.6. Mössbauer spectroscopy

^{197}Au Mössbauer spectra were recorded with a source of ^{197}Pt in isotopically enriched ^{196}Pt metal. Both the source and absorber were kept at 4.2 K and an intrinsic Ge detector (1024 channels) was used for detecting the 77.3 keV γ-rays. The Mössbauer spectrometer was operated with a sinusoidal drive velocity waveform. ^{57}Fe Mössbauer spectra were measured with a source of ^{57}Co in an Rh matrix and a Kr/CO_2 proportional counter was used to detect the 14.4 keV γ-rays. Room temperature spectra were recorded using a Wissel MR-260 (576 channel) spectrometer operated with a triangular waveform. The ^{197}Au and ^{57}Fe spectra were calibrated against the Pt metal source and α-Fe, respectively. Both the ^{197}Au and ^{57}Fe spectra were computer analysed using a least-squares fitting programme based on superpositions of Lorentzian sextets, doublets and singlets under the thin absorber approximation. The validity of this approximation was verified by comparison with analysis using the full transmission integral. Spectral parameters including the isomer shift δ, the quadrupole splitting Δ or the quadrupole shift 2ε, the magnetic hyperfine field B_{hf} and the relative areas of the different components were thus determined.

3. Results

3.1. ICP and BET analysis

The Au contents of the three samples as determined by ICP analysis were 1.15, 1.44 and 2.10 at.%, respectively. The corresponding surface areas of the three samples after drying at 120 °C and again after calcination at 400 °C for 3 h are presented in Table 1. It

Table 1
Au content and BET surface areas of the gold/iron-oxide catalysts

Sample	at.% Au (ICP), dried material	BET surface area (m^2/g)	
		Dried material	Calcined material
a	1.15	218	38
b	1.44	240	47
c	2.10	253	40

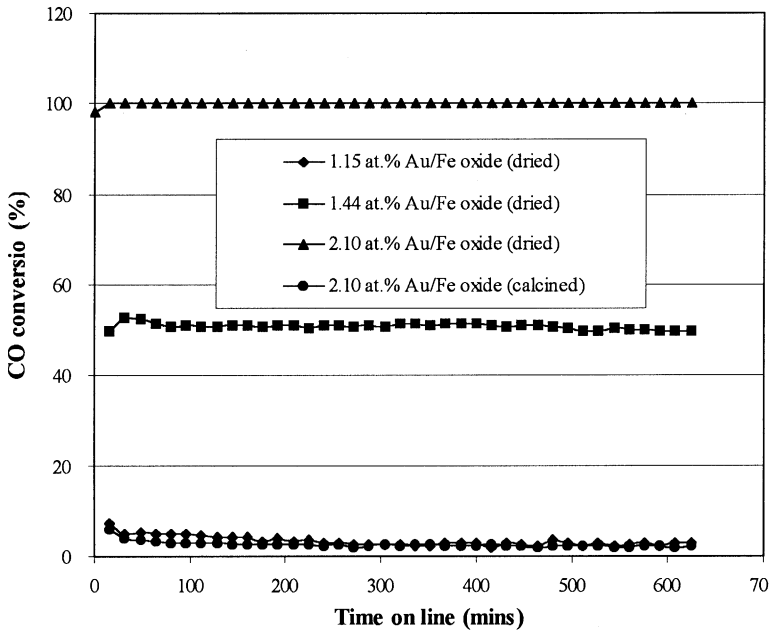

Fig. 1. CO conversion at 20 °C as a function of time-on-line for the dried and calcined portions of the gold/iron-oxide catalysts.

is clear that the materials dried at 120 °C have a high surface area (200–250 $m^2\ g^{-1}$) and show a slight trend of increasing surface area with increasing Au content. Following calcination, the surface area for all three samples collapses to between 38 and 47 $m^2\ g^{-1}$.

3.2. Catalytic performance

Fig. 1 shows the CO conversion versus the time-on-line for all three dried samples and the most active of the calcined materials (i.e. 2.10 at.% Au). It is clear that the dried 2.10 at.% Au sample shows by far the highest activity towards room temperature CO oxidation, rapidly attaining 100% conversion after 20 min on-line, and maintaining that for the full 10 h duration of the test. The 1.44 at.% Au and 1.15 at.% Au-dried samples reached considerably lower steady state conversions of around 50 and 3%, respectively. In fact, this decreasing level of activity with decreasing Au content and decreasing surface area for the dried samples closely mimics the trend reported in our previous publication [12], with the ~2 at.% Au level giving the best results. By comparison, all the gold/iron-oxide materials calcined at 400 °C for 3 h showed a very poor performance, displaying CO conversions of less than 4% for the entire duration of the test.

It is important to note that the 'pure' gold- and iron-oxide materials were also tested for low-temperature CO activity both before and after calcinations. All of the pure control samples exhibited less than 3% CO conversion, with the uncalcined materials having a poorer activity than their pure calcined counterparts. The inactivity of the uncalcined gold- and iron-oxide 'precursor' samples when physically separate, clearly demonstrates that a combination of the two materials creates a synergistic effect that is beneficial for low-temperature CO oxidation.

3.3. X-ray diffraction

Fig. 2 shows the XRD patterns obtained from the 1.15, 1.44 and 2.10 at.% Au-dried samples. They are all very similar and suggest that the dried material is extremely disordered in character. A few very broad bumps are replicated in all three patterns, but they cannot be convincingly assigned to any particular phase (e.g. ferrihydrite, goethite or haematite). The corresponding XRD patterns for the three materials

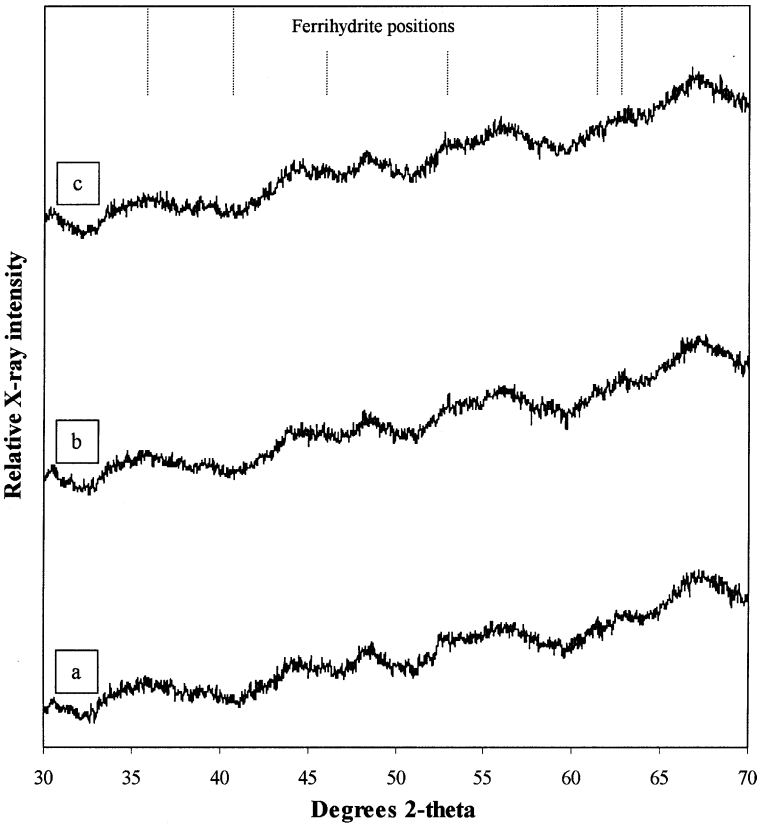

Fig. 2. X-ray diffraction powder patterns for gold/iron-oxide catalysts dried at 120 °C with: (a) 1.15 at.% Au, (b) 1.44 at.% Au and (c) 2.10 at.% Au.

calcined at 400 °C for 3 h are shown in Fig. 3. Again, the patterns look similar for all three samples. However, in this case distinct sharp peaks are visible which can be unequivocally indexed to the 012, 104, 110, 024, 116, 214 and 300 reflections of haematite (α-Fe_2O_3). A very weak reflection corresponding to the Au 1 1 1 lattice spacing is also possibly present.

3.4. Electron microscopy

Fig. 4 shows an HREM micrograph of the 2.10 at.% Au/ferric-oxide material dried at 120 °C. The microstructure shown was typical of that found for all the materials dried at 120 °C, observed both *before* and *after* catalyst testing. Micron scale agglomerates of particles ranging between 4 and 8 nm in diameter were observed. The phase contrast observed within individual particles was characteristic of a disordered or at best semi-crystalline material. Very occasionally nanocrystals of α-Fe_2O_3 were observed, such as that indicated in Fig. 4. However, such grains are probably artefacts since they can be generated by focussing the electron probe down to a stationary intense spot. The ensuing localised heating under a vacuum environment then causes a rearrangement of the disordered particle to crystalline α-Fe_2O_3. It is important to note that metallic Au nanocrystals were never observed in any of the dried specimens. This suggests that the Au is either atomically dispersed, or else is in a sub-nanometer particle form that is impossible to distinguish from the speckle contrast exhibited by the support. In order to try to assess the location of the Au in the sample, elemental X-ray mapping on an agglomerate in the 2.10 at.% Au-dried sample was

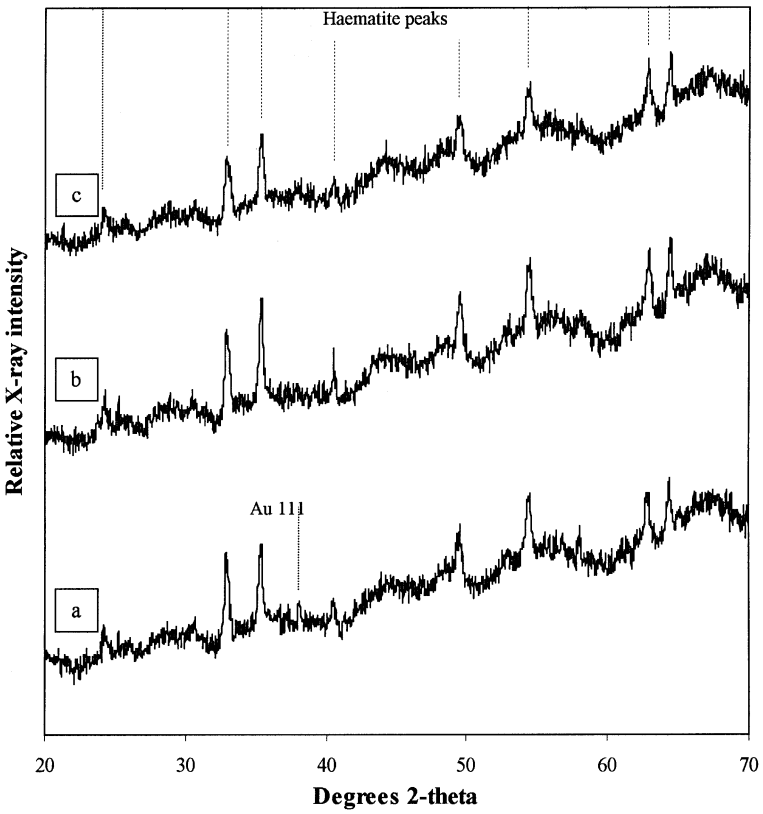

Fig. 3. X-ray diffraction powder patterns for the calcined gold/iron-oxide catalysts containing: (a) 1.15 at.% Au, (b) 1.44 at.% Au and (c) 2.10 at.% Au.

performed in an STEM, as shown in Fig. 5. Elemental maps using the Fe Kα_1 (6.404 keV), Au Mα_1 (2.123 keV) and O Kα_1 (0.525 keV) emission lines of the same area of specimen were obtained as shown. It is clear that all three constituent elements are homogeneously distributed throughout the agglomerate (i.e. the Au is not obviously segregating into discrete islands or rafts).

After calcination at 400 °C, the materials develop a very different microstructure as illustrated in Fig. 6 for the 2.10 at.% Au sample. A dispersion of discrete metallic Au nanoparticles having typical diameters of 3–5 nm are clearly visible. They are supported on highly crystalline α-Fe_2O_3 grains that are typically about 20 nm in size. Such an observation correlates well with the measured drop of surface area from 218 $m^2\,g^{-1}$ in the dried form to 38 $m^2\,g^{-1}$ in the calcined state. HREM images such as that presented in Fig. 7 demonstrate that the Au particles predominantly have a cuboctahedral morphology and preferentially expose {1 1 1} and {1 0 0}-type surface facet planes.

3.5. Mössbauer spectroscopy

^{197}Au Mössbauer spectra of all the dried samples are shown in Fig. 8, whereas those for the corresponding calcined materials are presented in Fig. 9. The associated spectral parameters derived from these ^{197}Au Mössbauer spectra are summarised in Table 2. It is clear that the calcined samples (Fig. 9) resemble each other in having one main absorption peak at a negative velocity typical of metallic Au, i.e. they exhibit a singlet spectrum with an isomer shift of around -1.23 mm s^{-1}. This observation is fully consistent with the electron microscopy studies, confirming that

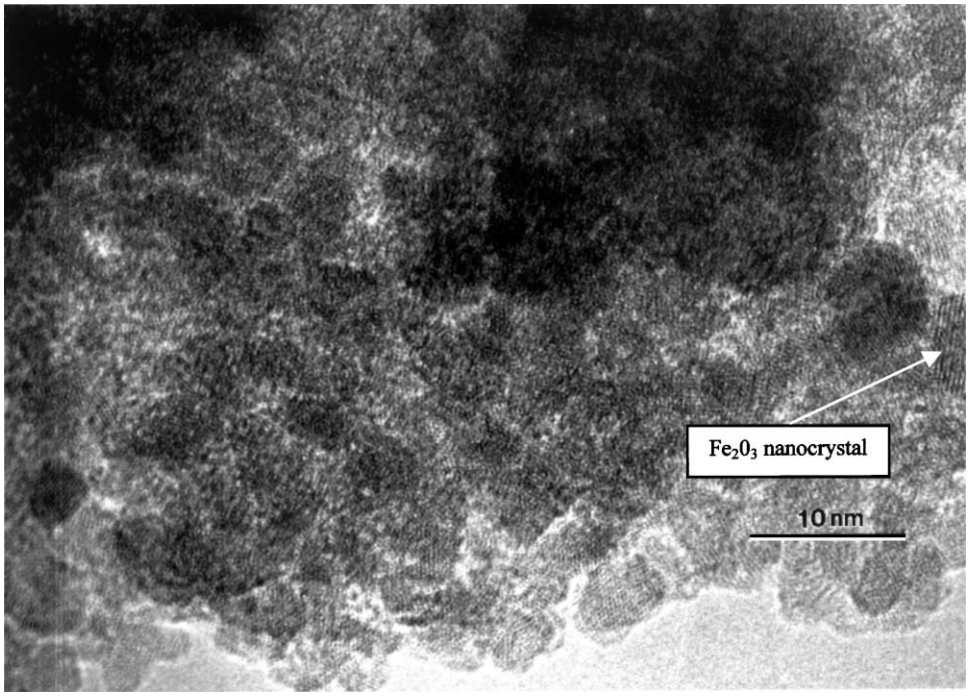

Fig. 4. HREM micrograph of 2.10 at.% gold/iron-oxide material dried at 120 °C.

metallic Au species have been formed by the 400 °C calcination treatment. By way of comparison, the ^{197}Au Mössbauer spectra of the dried series of samples (Fig. 8) all showed two peaks, but with varying proportions. The first symmetric peak at a velocity of $-1.23\,\mathrm{mm\,s^{-1}}$ can be once again be ascribed to the presence of metallic Au. The second peak, however, which is asymmetric in shape and has a maximum in the range 1–1.3 $\mathrm{mm\,s^{-1}}$ can be attributed [11] to Au(III) oxyhydroxide ($AuOOH{\cdot}xH_2O$). The relative areas of these two peaks as function of Au content are also listed in Table 2. The dried materials having

Table 2
^{197}Au Mössbauer spectroscopy parameters for gold/iron-oxide catalysts measured at 4.2 K

Catalyst	Isomer shift, δ (mm/s)	Quadrupole splitting, Δ (mm/s)	Relative spectral area, A	Phase assignation
Samples dried at 120 °C				
1.15 at.% Au/Fe-oxide	−1.22	–	86	Au metal
	1.33	1.35	14	$AuOOH{\cdot}xH_2O$
1.44 at.% Au/Fe-oxide	−1.24	–	80	Au metal
	0.98	1.19	20	$AuOOH{\cdot}xH_2O$
2.10 at.% Au/Fe-oxide	−1.23	–	40	Au metal
	1.30	1.71	60	$AuOOH{\cdot}xH_2O$
Samples calcined at 400 °C				
1.15 at.% Au/Fe-oxide	−1.20	–	100	Au metal
1.44 at.% Au/Fe-oxide	−1.22	–	100	Au metal
2.10 at.% Au/Fe-oxide	−1.20	–	100	Au metal

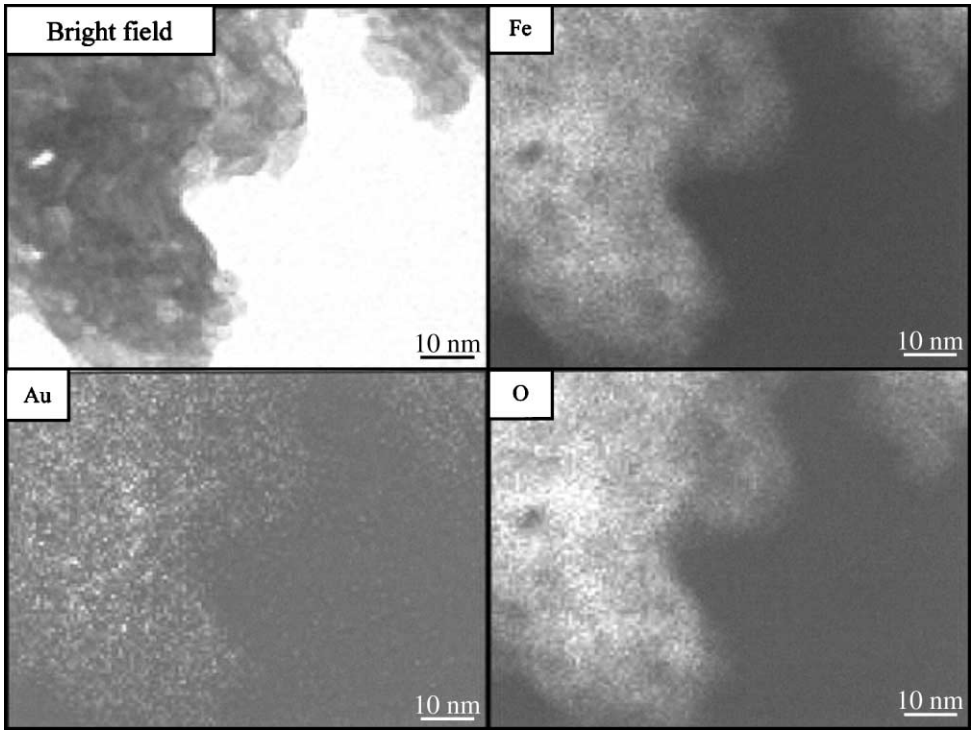

Fig. 5. Bright field STEM image and Fe, Au and O energy dispersive X-ray maps of a region of the 2.10 at.% Au/ferric-oxide material (dried at 120 °C) using the Fe $K\alpha_1$, Au $M\alpha_1$ and O $K\alpha_1$ peaks at X-ray energies of 6.404, 2.123 and 0.525 keV, respectively.

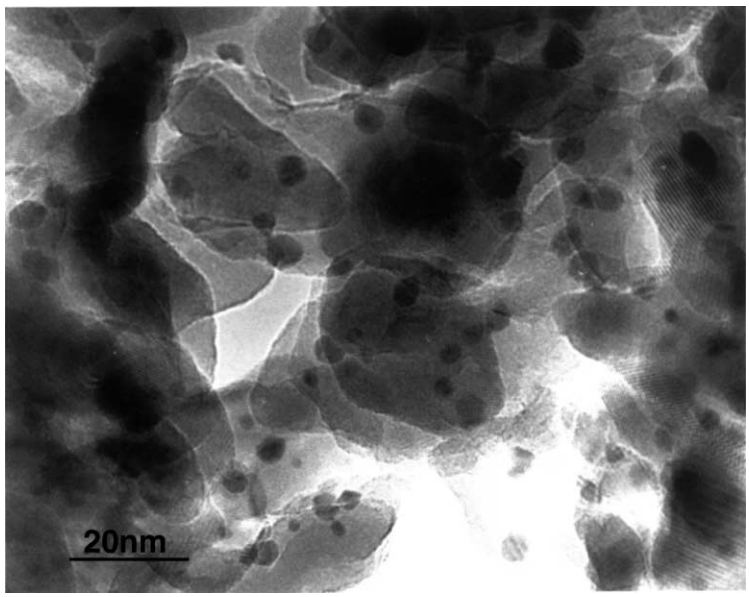

Fig. 6. TEM micrograph showing the dispersion of nanometer scale Au particles on α-Fe_2O_3 in the 2.10 at.% sample calcined at 400 °C.

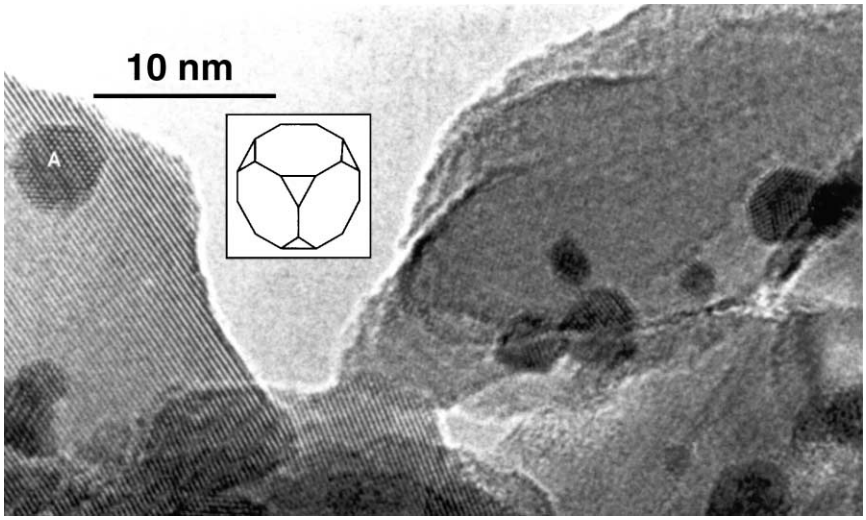

Fig. 7. HREM micrograph showing the morphology of Au particles in the 2.10 at.% gold/iron-oxide sample calcined at 400 °C. A schematic representation of a truncated cube octahedral particle viewed along the [1 1 1] direction is shown in the inset.

1.15 and 1.44 at.% Au were comprised mainly of metallic Au species and only contained 14 and 20% of Au in oxidised form, respectively. By way of contrast, the 2.10 at.% Au-dried sample contained a much higher fraction (60%) of the Au(III) oxyhydroxide phase. In fact, the increasing $AuOOH{\cdot}xH_2O$ component in the dried sample seems to correlate with increasing Au content and improved CO conversion.

The ^{57}Fe Mössbauer spectra (acquired at 293 K) of all the dried and the calcined samples are presented in Fig. 10, along with the corresponding spectral parameters which are shown in Table 3. All the calcined samples show a sharp magnetic sextet with Δ and 2ε parameters that are consistent with well-crystallised haematite (α-Fe_2O_3). The ^{57}Fe Mössbauer spectra of all the dried materials are dominated by a paramagnetic doublet at 293 K that collapses to a broadened sextet at 4.2 K. Such superparamagnetic behaviour and the associated hyperfine parameters are completely consistent with the presence of a ferrihydrite ($Fe_5HO_8{\cdot}4H_2O$) phase [11].

Table 3
^{57}Fe Mössbauer spectroscopy parameters for gold/iron-oxide catalysts measured at 293 K

Catalyst	Isomer shift, δ (mm/s)	Δ[a] (mm/s)	Hyperfine field, B_{hf} (T)	Relative spectral area, A	Phase assignation
Samples dried at 120 °C					
2.10 at.% Au/Fe-oxide	0.34	0.68	–	100	Ferrihydrite
1.44 at.% Au/Fe-oxide	0.35	0.69	–	100	Ferrihydrite
1.15 at% Au/Fe-oxide	0.34	0.70	–	100	Ferrihydrite
		2ε[a] (mm/s)			
Samples calcined at 400 °C					
2.10 at.% Au/Fe-oxide	0.37	−0.22	50.2	100	Haematite
1.44 at.% Au/Fe-oxide	0.37	−0.20	50.4	100	Haematite
1.15 at.% Au/Fe-oxide	0.37	−0.21	50.4	100	Haematite

[a] This column contains either the quadrupole splitting, Δ (mm/s), for the doublet spectra or the quadrupole shift, 2ε (mm/s), for the sextet subspectra.

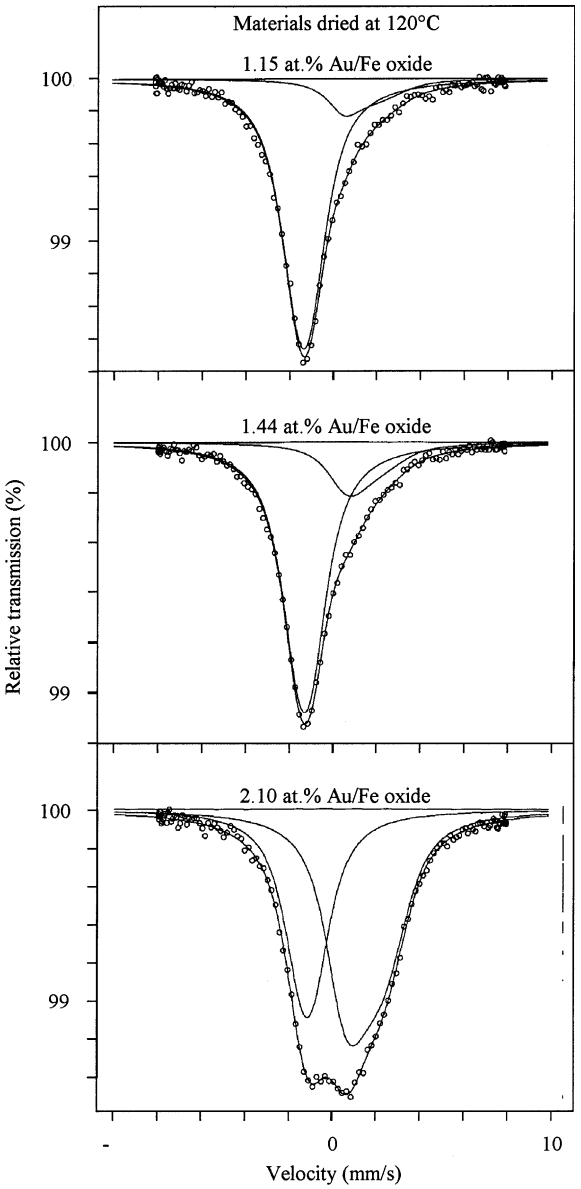

Fig. 8. ^{197}Au Mössbauer spectra for gold/iron-oxide catalysts dried at 120 °C, measured at 4.2 K.

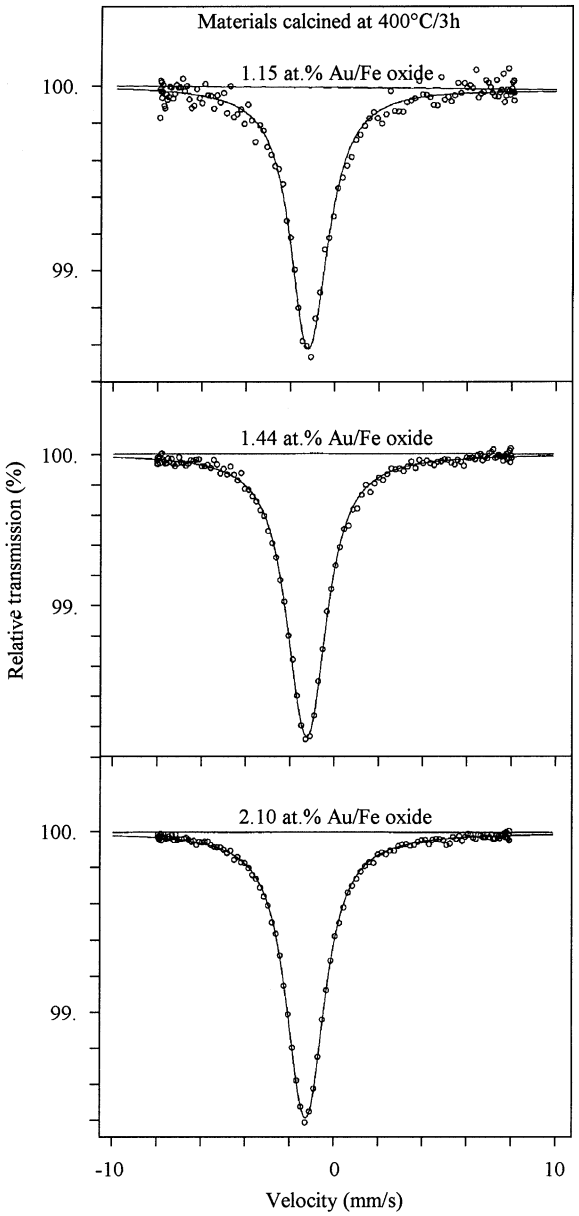

Fig. 9. ^{197}Au Mössbauer spectra for gold/iron-oxide catalysts calcined at 400 °C for 3 h, measured at 4.2 K.

4. Discussion

It is apparent from our microstructural characterisation that the precursor materials dried at 120 °C are very different from the corresponding catalysts after calcination at 400 °C. The calcined materials are comprised solely of 3–5 nm cuboctahedral metallic Au particles supported on 20 nm diameter well-crystalline α-Fe_2O_3 particles. By comparison the dried materials consist of micron scale agglomerates of 4–8 nm disordered ferrihydrite particles on which the Au

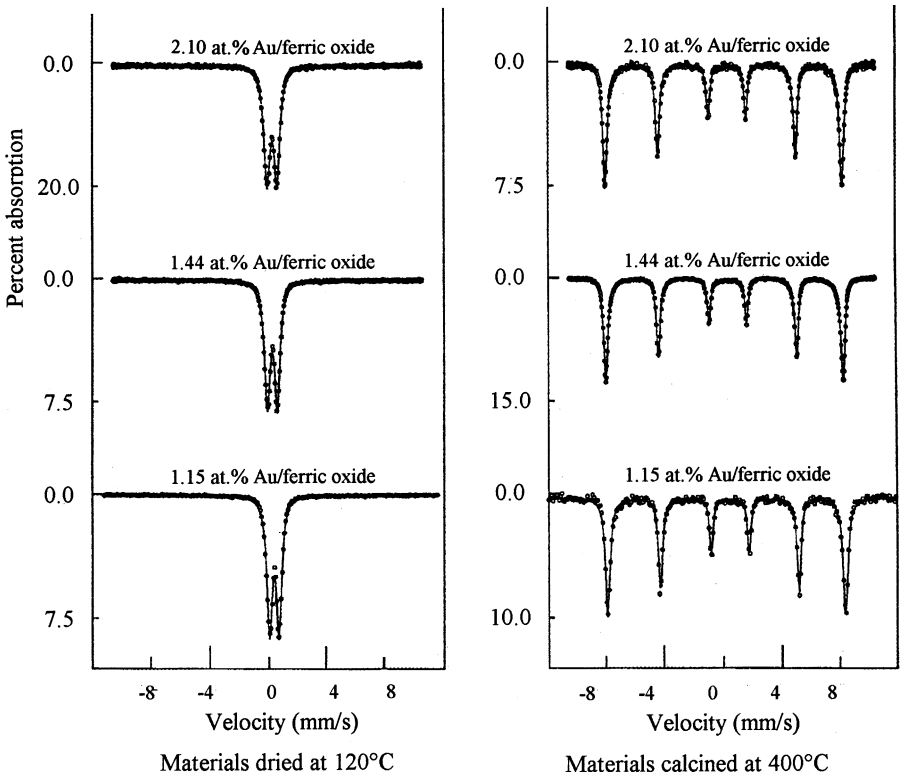

Fig. 10. ^{57}Fe Mössbauer spectra for the calcined and uncalcined gold/iron-oxide catalysts measured at 293 K.

is uniformly dispersed in the form of a mixture of $AuOOH{\cdot}xH_2O$ and Au^0.

In our work, the drying temperature of 120 °C during catalyst preparation assumes critical significance when considered in the light of the known chemistry of gold-oxide. As documented in Sidgwick [13] (and subsequently in abbreviated form in many standard inorganic chemistry texts), gold oxyhydroxide may be obtained from aqueous solutions of Au(III) by precipitation with alkali, and purified by dissolution in excess alkali, presumably as $[Au(OH)_4]^-$, followed by reprecipitation [14]. When dried over phosphorus pentoxide it forms a brown powder of composition Au(O)OH which, after prolonged heating at 140–150 °C, loses water to give first, Au_2O_3 which is also brown, and at slightly higher temperatures (ca. 160 °C), the poorly characterised Au_2O; at significantly higher temperatures decomposition to metallic gold occurs. Haruta et al. [15] have also presented results obtained by EXAFS on how gold species in Au–Fe co-precipitated precursors change after drying and calcining at different temperatures. They showed that hydrous gold species can be stabilised in the matrix of ferric hydroxide even up to 300 °C and that heating up to 400 °C causes almost all oxidic species to be decomposed into metallic ones.

When tested for low-temperature CO oxidation, all the calcined materials were relatively inactive. At first sight, this behaviour seems contrary to the conventional wisdom that 2–5 nm supported Au particles on a metal-oxide support are beneficial because of the optimised length of interfacial perimeter that they expose. However, when considered in the context of the Bond and Thompson model [5], their inactivity may well be related to the fact that: (i) the requisite *mixture* of Au^0 and Au^{x+} species is absent, and (ii) the oxide support may be *too* perfect leading to a deficiency in active superoxide species.

The dried materials when tested for low-temperature CO oxidation showed greater variations in their catalytic behaviour. The most active material, containing 2.1 at.% Au (40% Au^0:60% Au^{3+}), exhibited 100% CO conversion after 20 min on-line, and maintained that level of activity for the full 10 h duration of the test. The next best dried material (1.44 at.% Au with 80% Au^0:20% Au^{3+}) exhibited a CO conversion of around 50%. Finally, the 1.15 at.% Au-dried sample (with 86% Au^0:14% Au^{3+}) exhibited a behaviour which was just marginally better than the calcined materials. These observations are consistent with the Bond and Thompson model [5] in that those catalysts displaying good CO conversion definitely contained *mixtures* of Au^{x+} and Au^0 species. In addition, these results suggest that the precise Au^{x+}/Au^0 ratio in the material may have an important effect on the level of catalytic activity displayed. It should be noted, however, that the precise location of the Au^0 sites with respect to the Au^{3+} sites still needs to be elucidated for these rather complex disordered Au oxyhydroxide/Au/ferrihydrite systems.

Date and Haruta [16] have recently investigated the effect of moisture on CO oxidation over the related Au/TiO_2 system. Low levels of moisture were found to enhance the reaction by an order of magnitude, whereas higher moisture levels actually suppressed the reaction. The authors also noted that the amount of moisture absorbed on the catalyst influences the activity more than the moisture content of the gas phase, which led them to infer that the low-temperature CO oxidation over the gold catalyst involved water derived species on the catalyst surface. Hence in our case it is also tempting to associate the high activity of our $AuOOH{\cdot}xH_2O/Au/Fe_5HO_8{\cdot}4H_2O$ material with the high proportion of hydroxy groups and water incorporated into the ferrihydrite and gold oxyhydroxide.

Acknowledgements

We would like to thank the UK Engineering and Physical Sciences Research Council for their support, and the British Council and Deutscher Akademischer Austauschdienst for an Academic Research Collaboration grant. NAH is grateful to Johnson Matthey for financial support via a CASE studentship.

References

[1] M. Haruta, T. Kobayashi, H. Sano, N. Yamada, Chem. Lett. (1987) 405.
[2] M. Haruta, N. Yamada, T. Kobayashi, S. Iijima, J. Catal. 115 (1989) 301.
[3] S.D. Lin, M. Bollinger, M.A. Vannice, Catal. Lett. 17 (1993) 245.
[4] H. Sakurai, M. Haruta, Catal. Today 29 (1996) 361.
[5] G.C. Bond, D.T. Thompson, Gold Bull. 33 (2000) 41.
[6] M.A.P. Dekkers, M.J. Lippits, B.E. Nieuwenhuys, Catal. Lett. 56 (1998) 195.
[7] M.A.P. Dekkers, M.J. Lippits, B.E. Nieuwenhuys, Catal. Today 54 (1999) 381.
[8] F. Boccuzi, A. Chiorino, S. Tsubota, M. Haruta, J. Phys. Chem. 100 (1996) 3625.
[9] F. Boccuzi, A. Chiorino, M. Mazoli, D. Andreeva, T. Tabakova, J. Catal. 188 (1999) 176.
[10] D.A.H. Cunnigham, W. Vogel, M. Haruta, Catal. Lett. 63 (1999) 43.
[11] F.E. Wagner, S. Galvagno, C. Milone, A.M. Visco, L. Stievano, S. Calogero, J. Chem. Soc., Faraday Trans. 93 (1997) 3403.
[12] R.W. Finch, N.A. Hodge, G.J. Hutchings, A. Meagher, Q.A. Pankhurst, M.R.H. Siddiqui, F.E. Wagner, R. Whyman, Phys. Chem. Chem. Phys. 1 (1999) 485.
[13] N.V. Sidgwick, Chemical Elements and Their Compounds, Vol. 1, Clarendon Press, Oxford, 1950, p. 179.
[14] W.E. Roseveare, T.F. Buehrer, J. Am. Chem. Soc. 49 (1927) 1221.
[15] M. Haruta, S. Tsubota, T. Kobayashi, H. Kageyama, M.J. Genet, B. Delmon, J. Catal. 144 (1993) 175.
[16] M. Date, M. Haruta, J. Catal. 201 (2001) 221.